Embedded ultrasound sensor in a silicon-on-insulator photonic platform

Amir Rosenthal, Murad Omar, Hector Estrada, Stephan Kellnberger, Daniel Razansky, Vasilis Ntziachristos
Citation: Applied Physics Letters **104**, 021116 (2014); doi: 10.1063/1.4860983
View online: http://dx.doi.org/10.1063/1.4860983
View Table of Contents: http://scitation.aip.org/content/aip/journal/apl/104/2?ver=pdfcov
Published by the AIP Publishing

Embedded ultrasound sensor in a silicon-on-insulator photonic platform

Amir Rosenthal, Murad Omar, H_ector Estrada, Stephan Kellnberger, Daniel Razansky, and Vasilis Ntziachristos
Institute for Biological and Medical Imaging (IBMI), Technische Universität München and Helmholtz Zentrum München, Ingoldstädter Landstraße 1, 85764 Neuherberg, Germany

(Received 30 August 2013; accepted 16 December 2013; published online 15 January 2014)

A miniaturized ultrasound sensor is demonstrated in a silicon-on-insulator platform. The sensor is based on a p-phase-shifted Bragg grating formed by waveguide corrugation. Ultrasound detection is performed by monitoring shifts in the resonance frequency of the grating using pulse interferometry. The device is characterized by measuring its response to a wideband acoustic point source generated using the optoacoustic effect. Experimental results show that the sensor's response is dominated by the formation of surface acoustic waves.

Silicon-on-insulator (SOI) technology holds great promise for the development of miniaturized optical sensors that may be seamlessly integrated with other silicon-based devices. SOI optical-waveguide technology has been applied to biological[1–3] and chemical[4–6] sensing by exposing the evanescent part of the guided mode to the substance of interest.[7] In such geometries, refractive index changes on the waveguide's surface—whether caused directly by the presence of the measurands[1] or mediated by labeling (Ref. 8)—affect the phase velocity of the guided mode, enabling interferometric detection. SOI sensors have also been demonstrated for detecting pressure,[9] strain,[10–12] and temperature.[13] In those applications, the waveguide is fully embedded in a solid cladding, and the sensing mechanism is based on the deformation of the waveguide and variations in the core's refractive index. Since ultrasound is essentially a mechanical deformation wave, such mechanical sensors are also appropriate for ultrasound sensing, as previously noted in Ref. 12. Nonetheless, no experimental demonstration of ultrasound detection using SOI photonic devices has so far been achieved.

Although numerous optical techniques exist for ultrasound detection, relatively few are based on sensors integrated in optical waveguides. These include Mach-Zehnder fiber interferometers,[14] fiber-based Fabry-Perots,[15] uniform fiber Bragg gratings (FBGs),[16] π-phase-shift fiber Bragg gratings (π-FBGs),[17,18] uniform polymer Bragg grating waveguides,[19] and micro-rings produced in a polymer-waveguide platform.[20,21] π-FBGs and polymer-based micro-rings currently represent the most compact waveguide-embedded ultrasound sensors in fiber and planar geometries, respectively, where π-FBGs are characterized by a typical length of 300 μm and diameter of 10 μm, and micro-rings have so far achieved a diameter of 100 μm and thickness of approximately 2 μm in the telecom wavelengths.[20,21] Although the miniaturization level demonstrated for waveguide-embedded sensors in recent years enables the detection of high-frequency ultrasound and could facilitate imaging applications, it has not reached the level achieved by capacitive micro-machined ultrasonic transducers (CMUT), where transducers with diameters as small as 15 μm have been demonstrated.[22] Theoretically, in both π-FBGs and micro-rings, further sensor miniaturization can be achieved by increasing the refractive-index differences employed, making the SOI platform attractive for the miniaturization of optical sensors of ultrasound. Experimentally, the implementation of micro-rings[23] and π-FBGs[24] in SOI for optical filtering applications has demonstrated significant reduction in the size of these components compared to the level achieved in polymer- or glass-based waveguides.

In this Letter, we demonstrate a miniaturized wideband ultrasound sensor implemented in a SOI platform. The sensor is based on a π-phase shifted waveguide Bragg grating (π-WBG) produced by applying side corrugation to a silicon nanowire waveguide embedded in silica. The sensor was produced on a silicon wafer with the orientation (100). The fabrication and packaging of the sensor was performed via the ePIXfab service and TeraXion, Inc. (Quebec, Canada). Similarly to the π-FBG sensor demonstrated in Refs. 17 and 18, ultrasound sensing with the π-WBG sensor is based on monitoring shifts in its resonance wavelength, and light localization around the π-phase shift leads to an effective sensor length significantly smaller than the physical length of the π-WBG.

Figure 1(a) shows a schematic top-view description of the π-WBG, where $w = 500$ nm is the waveguide width, $\Delta w = 40$ nm is the corrugation depth, $L = 250\,\mu$m is the length of the grating, and $\Lambda = 320$ nm is the period length. A cross-section of the silicon nanowire waveguide and the wafer is given in Fig. 1(b). To enable easy handling of the silicon die, whose lateral dimensions were 6 mm and 10 mm, it was permanently bonded on the side of the silicon substrate to a large polymer substrate with lateral dimensions of 6 cm and 10 cm and a thickness of 6 mm, which functioned as a holder. The device was fiber-coupled on both its sides to side-polished polarization-maintaining fibers by the use of grating couplers, similarly to Ref. 25. To enable the under-water reflection of light from the fiber's core to the grating coupler and vice versa, a reflective coating was applied to the side-polished fiber tips. In contrast, in Ref. 25 no reflective coating was used, and reflection was based solely on the total internal reflection between glass and air, limiting under-water applications. Figure 1(c) shows an illustration of the fiber coupling. The transmission spectrum of the π-WBG is shown in Fig. 1(d). The figure shows a 10 dB loss due to coupling

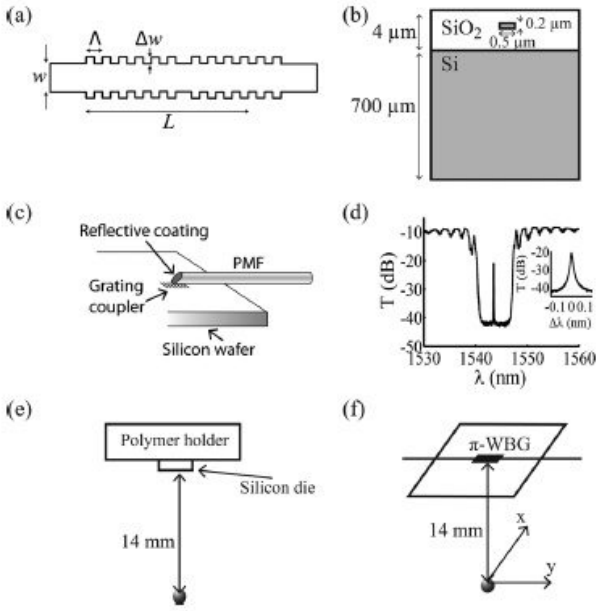

FIG. 1. (a) A schematic, top-view description of the π-WBG (not to scale). $w = 500$ nm is the waveguide width, $\Delta w = 40$ nm is the corrugation depth, $L = 250\ \mu$m is the length of the grating, and $\Lambda = 320$ nm is the period length. (b) A cross-sectional view of the SOI waveguide. (c) An illustration of the fiber coupling to the π-WBG. (d) The transmission spectrum of the connectorized π-WBG device. The inset shows the transmission notch magnified. (e), (f) Schematic drawings depicting the acoustic-characterization experiment for the π-WBG sensor.

losses and an additional 10 dB loss at the notch wavelength, which may be attributed to losses in the waveguide and to manufacturing errors. The 3 dB bandwidth of the notch was approximately 13 pm.

To evaluate the performance of the π-WBG as an ultrasound sensor, we employed the acoustic characterization technique used in Ref. 18. Briefly, an acoustic point source was generated in a water tank via the optoacoustic effect by illuminating a dark polyethylene microsphere with an approximate diameter of 100 μm (Cospheric LLC, Santa Barbara, California) with 8 ns optical pulses delivered at a rate of 20 Hz with a wavelength of 532 nm and average power of 200 mW (laser model: VIBRANT Arrow 532 type I, Opotek, Carlsbad, CA, USA). Similarly to Refs. 18 and 26, the microsphere was embedded in transparent agar, which served as a holder. As shown in Fig. 1(e), the polymer sensor holder was positioned in the water tank with an approximate distance of 14 mm between the microsphere and the silica surface of the detector. The holder was scanned laterally over the x and y axes shown in Fig. 1(f), whereas the microsphere position and illumination were kept constant to minimize temporal changes in the amplitude of the acoustic source. The y axis denotes the direction parallel to the waveguide whereas the x axis is perpendicular to the waveguide. The coordinate $(x,y) = (0,0)$ denotes the position for which the π-WBG is positioned directly above the microsphere. Because of technical constraints, the scan over the x -axis was limited to a maximum value of approximately $x = 2.5$ mm. Sensor interrogation, i.e., monitoring of shifts in the notch wavelength due to ultrasound, was performed

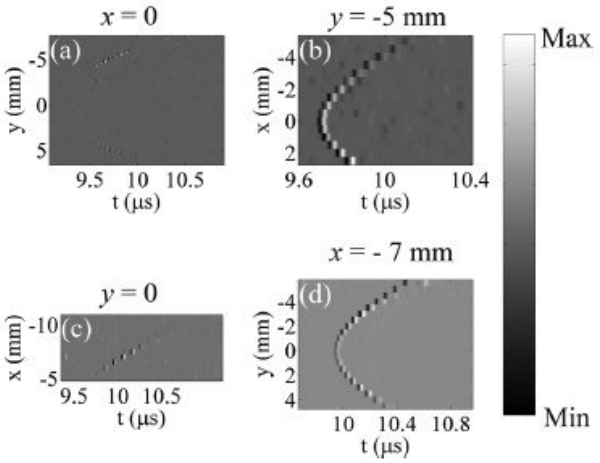

FIG. 2. The signals obtained for four linear scans of the sensor. The vertical axis of the graphs shows the position over which the acoustic sensor was scanned; the horizontal axis shows measurement time, and the gray color scale corresponds to the signal amplitude.

using pulse interferometry.[27] For each scan position, the signal was averaged 100 times to increase sensitivity.

Figure 2 shows the acoustic signals measured for linear scans of the acoustic point source. The vertical axis of the graphs shows the position over which the acoustic sensor was scanned; the horizontal axis shows the measurement time; and the gray color scale corresponds to the signal amplitude. As shown in Fig. 2(a), for the y scan performed at $x = 0$, no signal could be detected at the coordinate (0,0), and the maximum signals were obtained symmetrically at $y = \pm 5$ mm, corresponding to an incident angle of approximately 19.7°. In order to examine the signal behavior around this angle, a linear scan in x was performed at $y = -5$ mm, whose results are shown in Fig. 2(b). Figure 2(c) shows the scan performed on $y = 0$. Because of the limitation in the scan on the x axis, it was not possible to measure the signal for x values larger than 2.5 mm and present a symmetric image similar to Fig. 2(a). Except for the signals shown in Fig. 2(c), no other signals could be observed in that measurement. The maximum signal was obtained at a position of $x = -7$ mm, which corresponds to an angle of approximately 26.6°. Figure 2(d) shows the corresponding y scan at the position $x = -7$ mm. The position of the coordinate $(x,y) = (0,0)$ in Fig. 2 was determined by requiring that signal delays exhibited in Figs. 2(b) and 2(d) be symmetric with offset. This position was in general agreement with visual inspection of the position of the microsphere relative to the silicon die.

The results presented in Fig. 2 are fundamentally different from those obtained for polymer-based optical sensors of ultrasound in planar geometries.[20,21] In such sensors, experimental results could be mostly explained by a simple model which accounts only for propagation effects in homogeneous medium and for the geometries of the sensor and source. In such a simplified model, the maximum signal amplitude should be obtained at the coordinate $(x,y) = (0,0)$ and gradually decrease with offset, clearly in contradiction to the results shown in Fig. 2. The qualitative behavior observed in Fig. 2 may be understood, however, in the context of Rayleigh waves, often referred to as surface acoustic waves

(SAWs). Specifically, it is well known that solid-liquid interfaces support leaky Rayleigh waves, which may be excited by an incident wave in the liquid with a certain angle of incidence that depends on the mechanical properties of the solid and the fluid.[28,29]

The results shown in Figs. 2(a) and 2(c) were used to calculate the velocity of the guided waves. For each dataset, the delay was calculated for the maximum of the signal for each position in which the signal could be distinguished from noise. The dependence of the delays on the positions is shown in Figs. 3(a) and 3(b) for the scans on the y and x axes, respectively, where linear fitting reveals the velocities of the Rayleigh waves, which are 4800 m/s and 5100 m/s, respectively. These values generally agree with previous numerical[29] and experimental[30] studies, where values ranging from 4756 m/s to 5200 m/s have been obtained for various configurations based on silicon substrates. These velocities may be used to calculate the Rayleigh critical angle, which is the incidence angle for which Rayleigh waves are excited and is given by[29]

$$\theta_{cr} = \sin^{-1} V_L / V_R, \tag{1}$$

where V_L and V_R are the acoustic velocity in the fluid (approximately 1500 m/s for water) and the velocity of the Rayleigh wave, respectively.

Based on the measured Rayleigh-wave propagation velocities and Eq. (1), the expected Rayleigh critical angles are 18.2° and 17.1° for the y and x scans, respectively, whereas the experimental values obtained from Fig. 2 are 19.6° and 26.6°. However, the experimental values correspond to the angle between the holder and the source, which should not necessarily be equal to the angle between the sensor and the source. The considerable discrepancy found for the x scan may be attributed to a relative tilt between the silicon die and the holder due to uneven bonding. In the case of the y scan, the symmetry found in Figs. 2(a) and 2(d) indicates that the scan plane and die were relatively parallel, validating the agreement between the two values of the Rayleigh critical angle. In the case of the x scan, parallelism, or lack thereof, could not be verified from Fig. 2(c) due to the limited scan range of the system whereas the signal Fig. 2(b) does not exhibit the symmetric behavior in amplitude found in Fig. 2(d), indicating a possible tilt on that axis. Therefore, the available measurement data does not enable a definite determination of the Rayleigh critical angle in the x direction.

Figure 3(c) shows the spectrum of the maximum signals obtained on the x and y scans in Figs. 2(a) and 2(c). The results generally show good agreement between the two spectra. We note that the bandwidths shown in Fig. 3(c) were the largest ones attained in our measurements. The spectra of the weaker signals in Figs. 2(a) and 2(c) exhibited smaller bandwidths owing to the larger attenuation of high frequency ultrasound. Theoretically, a polyethylene microsphere with a diameter of 100 μm should generate a spectrum which exhibits a main lobe with a maximum at 15 MHz and a cut-off frequency of 30 MHz, followed by side bands at higher frequencies.[18] The deviation of the measured spectra from the ideal may be a result of deformation of the microsphere due to the high-power laser pulses used for excitation

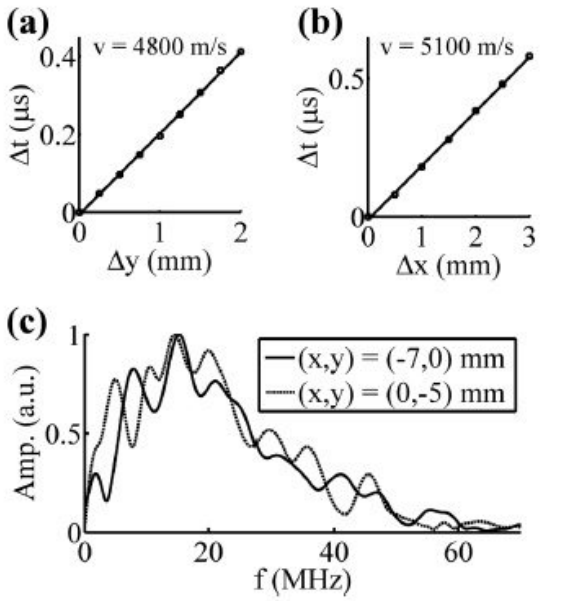

FIG. 3. The dependency of the signal delay on the offset in the (a) y and (b) x directions, where linear fitting was used to find the velocities in these directions. (c) The spectrum of the acoustic signals detected by the sensor at offsets on the x axis (solid curve) and y axis (dashed curve).

or defects on the surface of the wafer. We note that because pulse interferometry was used for interrogation with a 100 MHz repetition-rate pulse laser, the response at frequencies above 50 MHz could not be determined due to aliasing.[27] Additionally, aliasing of high-frequency signal components to low frequencies could explain the deviation of the measurement results from the theoretical spectra.

The similar spectral features obtained for the two propagation directions in Fig. 3(c) indicate that, similarly to π-FBG sensors,[17,18] the *effective* length of the sensor is smaller than its physical length. Based on an approximate phase velocity of 5000 m/s and maximum detected frequency of 50 MHz, the smallest wavelength of the Rayleigh waves obtained in the experiment is 100 μm. However, the length of the π-WBG is 250 μm, which corresponds to a Rayleigh wave with a frequency of 20 MHz. Because of spatial averaging, a detector of such a length would exhibit a significantly stronger drop in sensitivity at frequencies above 20 MHz for waves propagating in the y direction than it would for waves propagating in the x direction. Thus, the measured acoustic spectra indicate that the effective length of the ultrasound sensor is 100 μm or shorter. Theoretically, the effective length of π-WBG sensors is approximately equal to the inverse of their coupling coefficient κ.[17] Based on the analysis performed in Ref. 31, where the coupling coefficient of a π-WBG with an identical geometry was found to equal $\kappa = 288\ \mathrm{cm}^{-1}$, the theoretically expected effective length for the sensor is approximately 35 μm, i.e., an order of magnitude smaller than the values reported for π-FBG sensors.[17,18]

In conclusion, an embedded ultrasound sensor was demonstrated in an SOI platform. The sensor was based on a π-WBG created by side corrugation of a silicon nanowire optical waveguide. The acoustic response of the sensor in water was characterized using a point-like acoustic source generated by the optoacoustic effect and pulse interferometry for sensor

interrogation. The results indicate that the response of the sensor is mostly dominated by the formation of Rayleigh waves on the surface of the silicon wafer. The velocities measured in the characterization experiments are in general agreement with the values found in the literature. We note that since the thickness of the silica layer was considerably smaller than the wavelength of the Rayleigh waves, the propagation velocity was mostly determined by the mechanical properties of the silicon substrate.[29]

The performance demonstrated in this Letter suggests that the SOI π-WBG sensor may be used in SAW-based devices for monitoring their performance. Specifically, the sensor may be seamlessly integrated in existing SAW platforms based on Si-SiO_2 (Refs. 32 and 33) and generate valuable feedback about their operation, enabling design optimization. Based on the dimensions of the sensor and its coupling coefficient, it may be used to detect SAWs with frequencies up to approximately 140 MHz and 10 GHz for the x and y propagation directions, respectively. These frequencies make the π-WBG sensor compatible with SAW devices used in electronics[34] as well as in microfluidics.[35]

Finally, we note that in addition to applications in SAW devices, the proposed sensor could potentially be used for imaging, where a relatively broad detection angle is often required. Optical sensors in which the sensing elements are fabricated on the *surface* of silicon[19–21] or silica[36] substrates, rather than being embedded in silica, are not dominated by Rayleigh wave, and have shown to enable imaging applications. Therefore, a re-design of the cladding of the π-WBG sensor in which the waveguide is fabricated on the surface of the silica layer and is either exposed to the outer medium or covered by a polymer cladding may be compatible with imaging applications. Such cladding designs are common in SOI sensors used for biological and chemical applications[1–7] and therefore may be readily applied for acoustic sensing.

D.R. acknowledges support from the European Research Council Starting Grant; V.N. acknowledges support from the European Research Council through an Advanced Investigator Award.

[1]K. De Vos, I. Bartolozzi, E. Schacht, P. Bienstman, and R. Baets, Opt. Express **15**, 7610 (2007).
[2]K. De Vos, J. Girones, T. Claes, Y. De Koninck, S. Popelka, E. Schacht, R. Baets, and P. Bienstman, IEEE Photon. J. **1**, 225 (2009).
[3]D. X. Xu, A. Densmore, A. Delâge, P. Waldron, R. McKinnon, S. Janz, J. Lapointe, G. Lopinski, T. Mischki, E. Post, P. Cheben, and J. H. Schmid, Opt. Express **16**, 15137 (2008).
[4]N. A. Yebo, P. Lommens, Z. Hens, and R. Baets, Opt. Express **18**, 11859 (2010).
[5]J. T. Robinson, L. Chen, and M. Lipson, Opt. Express **16**, 4296 (2008).
[6]V. M. N. Passaro, F.Dell'Olio, and F. De Leonardis, Sensors **7**, 2741 (2007).
[7]A. Densmore, D. X. Xu, P. Waldron, S. Janz, P. Cheben, J. Lapointe, A. Delâge, B. Lamontagne, J. H. Schmid, and E. Post, IEEE Photon. Technol. Lett. **18**, 2520 (2006).
[8]W. E. Moerner, Proc. Natl. Acad. Sci. U.S.A. **104**, 12596 (2007).
[9]E. Hallynck and P. Bienstman, IEEE Photon. J. **4**, 443 (2012).
[10]W. J. Westerveld, J. Pozo, P. J. Harmsma, R. Schmits, E. Tabak, T. C. van den Dool, S. M. Leinders, K. W. van Dongen, H. P. Urbach, and M. Yousefi, Opt. Lett. **37**, 479 (2012).
[11]D. Taillaert, W. Van Paepegem, J. Vlekken, and R. Baets, Proc. SPIE **6619**, 661914 (2007).
[12]J. Pozo, W. Westerveld, P. J. Harmsma, S. Yang, P. Bodis, R. Nieuwland, M. Lagioia, D. M. R. L. Cascio, J. Staats, R. Schmits, H. V. D. Berg, E. Tabak, K. Green, H. P. Urbach, L. K. Cheng, and M. Yousefi, in Transparent Optical Networks (ICTON) 2011: Proceedings of the 13th International Conference, Stockholm, Sweden, 26–30 June 2011.
[13]G. D. Kim, H. S. Lee, C. H. Park, S. S. Lee, B. T. Lim, H. K. Bae, and W. G. Lee, Opt. Express **18**, 22215 (2010).
[14]D. Gallego and H. Lamela, Opt. Lett. **34**, 1807 (2009).
[15]H. Grün, T. Berer, P. Burgholzer, R. Nuster, and G. Paltauf, J. Biomed. Opt. **15**, 021307 (2010).
[16]N. E. Fisher, D. J. Webb, C. N. Pannell, D. A. Jackson, L. R. Gavrilov, J. W. Hand, L. Zhang, and I. Bennion, Appl. Opt. **37**, 8120 (1998).
[17]A. Rosenthal, D. Razansky, and V. Ntziachristos, Opt. Lett. **36**, 1833 (2011).
[18]A. Rosenthal, M. A. A. Caballero, D. Razansky, and V. Ntziachristos, Opt. Lett. **37**, 3174 (2012).
[19]V. Govindan and S. Ashkenazi, IEEE Trans. Ultrason. Ferroelectr. Freq. Control **59**, 2304 (2012).
[20]S. W. Huang, S. L. Chen, T. Ling, A. Maxwell, M. O'Donnell, L. J. Guo, and S. Ashkenazi, Appl. Phys. Lett. **92**, 193509 (2008).
[21]S. W. Huang, T. Ling, S. Ashkenazi, and L. J. Guo, IEEE Trans. Ultrason. Ferroelectr. Freq. Control **56**, 2482 (2009).
[22]K. K. Park, O. Oralkan, and B. T. Khuri-Yakub, IEEE Trans. Ultrason. Ferroelectr. Freq. Control **60**, 1245 (2013).
[23]M. S. Nawrocka, T. Liu, X. Wang, and R. R. Panepucci, Appl. Phys. Lett. **89**, 071110 (2006).
[24]Y. Painchaud, M. Poulin, C. Latrasse, N. Ayotte, M. J. Picard, and M. Morin, in Bragg Gratings, Photosensitivity, and Poling in Glass Waveguides (BGPP) 2012: Proceedings of the 13th International Conference, Colorado Springs, Colorado, USA, 17–20 June 2011.
[25]B. W. Snyder and P. A. O'Brien, in *Reliability, Packaging, Testing, and Characterization of MOEMS/MEMS and Nanodevices XII, San Francisco, California, USA, 04-05 February 2013*, pp. 86140D.
[26]A. Rosenthal, V. Ntziachristos, and D. Razansky, IEEE Trans. Ultrason. Ferroelectr. Freq. Control **58**, 316 (2011).
[27]A. Rosenthal, D. Razansky, and V. Ntziachristos, Opt. Express **20**, 19016 (2012).
[28]D. Royer and E. Dieulesaint, *Elastic Waves in Solids I: Free and Guided Propagation* (Springer-Verlag, Berlin/Heidelberg/New York, 2000), Chap. 5.
[29]G. M. Crean and A. Waintal, J. Appl. Cryst. **19**, 181 (1986).
[30]T. Tachizaki, T. Muroya, O. Matsuda, Y. Sugawara, D. H. Hurley, and O. B. Wright, Rev. Sci. Instrum. **77**, 043713 (2006).
[31]Y. Painchaud, M. Poulin, C. Latrasse, and M. J. Picard, in Group IV Photonics (GFP) 2012: Proceedings of the 13th International Conference, San Diego, California, USA, 29–31 August 2012.
[32]M. S. Nieuwenhuizen and A. J. Nederlof, Sens. Actuators B Chem. **9**, 171 (1992).
[33]S. Büyükköse, B. Vratzov, D. Ataç, J. van der Veen, P. V. Santos, and W. G. van der Wiel, Nanotechnology **23**, 315303 (2012).
[34]R. Weigel, D. P. Morgan, J. M. Owens, A. Ballato, K. M. Lakin, K. Hashimoto, and C. C. W. Ruppel, IEEE Trans. Microw. Theory Tech. **50**, 738 (2002).
[35]L. Y. Yeo and J. R. Friend, Biomicrofluidics **3**, 012002 (2009).
[36]B. T. Cox and P. C. Beard, IEEE Trans. Ultrason. Ferroelectr. Freq. Control **54**, 394 (2007).